Design and Development of a Planar Electromagnetic Conveyor for the Microfactory

Neha Arora, Muneeb Ullah Khan, Laurent Petit, Frederic Lamarque, Christine Prelle

Design and Development of a Planar Electromagnetic Conveyor for the Microfatory

Neha Arora, Muneeb Ullah Khan, Laurent Petit, Frédéric Lamarque, and Christine Prelle

***Abstract*—This paper presents a planar electromag-netic conveyor for a microfactory. The uniqueness of the conveyor design lies in its arrangement of overlapped two-dimensional mesh coils in matrix configuration that enables to drive a mobile part over long strokes. The conveyor architecture includes a fixed part, which consists of 5×5 matrix design that has been fabricated on a multilayer printed circuit board. An analytical model that takes into account the electromagnetic and friction effects has been developed. A conveyor prototype has been fabricated and experimentally characterized in open-loop control. Linear and planar motions, positioning repeatability error, straightness error, and rotation have been experimentally measured. From experimental results, the proposed architecture enables long linear displacement strokes ($\leqslant$70 mm) and rotation ($\leqslant \pm$12.37°). In addition, a 12 mm/s speed can be achieved for the mobile part at a nominal current of 0.8 A.**

***Index Terms*—Conveyor, electromagnetic forces, microactuators, microfactory, permanent magnet (PM) motors.**

I. Introduction

IN RECENT years, the demand for miniature systems has rapidly risen in order to add functionalities in mechatronic systems while increasing their miniaturization constraints [1]. To aid the manufacturing of such miniature systems, the microfactory concept has been proposed. This concept enables to adapt the size of the production tool to the size of the manufactured products, which results in reduction of footprint, energy consumption, cost, and production time [2]. However, due to the reduced dimensions of microfactory, manual intervention is not simple and/or not always possible. The microfactory should then present a high flexibility and adaptability level in order to be able to adapt the manufacturing flow to the demand [3]. This is important in the case of highly customized microproducts. In this context, conveyor system represents a fundamental element in a microfactory because it ensures the transportation of miniature parts between the different working stations [4]. In order to ensure high flexibility and adaptability levels, conveyor system should then be able to adapt and reconfigure production flows without manual intervention [5].

In literature, numerous technological solutions have been applied for the development of conveyors. These solutions are often based on direct drives technology to eliminate/reduce adverse effects of backlash, assembly errors, or friction due to the mechanical joints [6]. Among these solutions, the main advantages of the conveyors based on pneumatic [7] and thermomechanical [8] actuation principle include high generated forces, while piezoelectric [9], [10] and electrostatic [11] actuation technologies deliver high precision levels. Furthermore, levitation of the moved object can be easily obtained with pneumatic [12], [13] and electromagnetic [14]–[16] actuation principles.

Considering the advantages of the electromagnetic actuation principle such as high speed, low cost, large travel range, wire-free mobile part, etc., a compact micropositioning system capable to deliver millimeter level displacement strokes in xy plane has been developed [17]. Compared to conventional architecture of the planar systems that are often based on assembly of linear/rotation displacement stages, a parallel-kinematic configuration was selected to assemble four electromagnetic linear motors that resulted in the advantages such as low inertia, no cumulative error, and identical dynamic characteristics along working axes, etc., [18]. Apart from its ability to deliver nanometer level precision and millimeter level displacement range, the travel range of the system is limited to 10 mm in xy plane. This displacement range is sufficient for micro applications such as cell manipulation beneath a microscope, chip assembly, surface scanning, etc. However, in the context of microfactory, where long range ($>$10 mm) motion is often desired, such system cannot be adapted for conveyance tasks. So, in order to increase the travel range, one solution could be to enlarge the fixed part [see Fig. 1(a)]. However, this solution is unsuitable to drive multiple conveyors (e.g., conveyor P_1 and P_2) independently on a microfactory platform. In addition, the high resistance of drive coils due to its excessive length of the planar drive coils can increase Joule heating. This can deteriorate the miniature permanent magnets (PM) assembled in the mobile cross structure part of the conveyors.

Alternatively, a matrix configuration that consists of multiple drive cells is proposed to transport micro-objects across

This work was realized under the MICROCOSM Project and was supported in part by the Pi-cardie region and in part by Europe/FEDER with the European funds for regional developments at Picardie region of France. *(Corresponding author: Muneeb Ullah.)*

The authors are with the Roberval Laboratory FRE UTC-CNRS 2012, Sorbonne Universités, Université de Technologie de Compiègne, 60203 Compiègne, France (e-mail: neha.arora@utc.fr; muneeb-ullah.khan@utc.fr; laurent.petit@utc.fr; frederic.lamarque@utc.fr; christine.prelle@utc.fr).

This paper has supplementary downloadable material available at http://ieeexplore.ieee.org, provided by the authors.

Color versions of one or more of the figures in this paper are available online at http://ieeexplore.ieee.org.

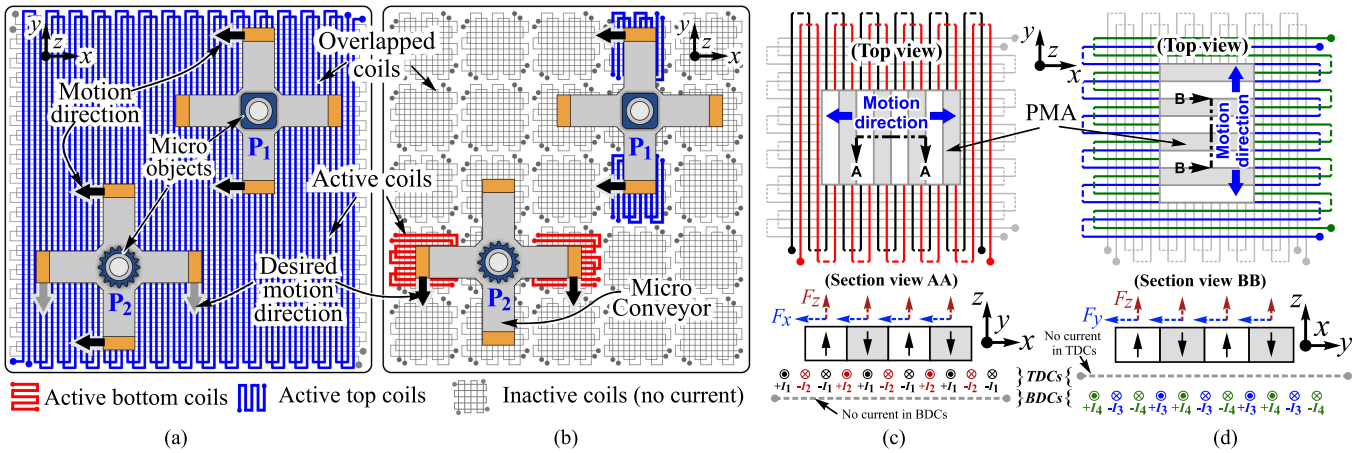

Fig. 1. Electromagnetic conveyor multilayer serpentine coils with (a) single mesh configuration and (b) multiple mesh matrix configuration. Working principle of the conveyor where the mobile PMA moves (c) along *x*-axis when TDCs are active and BDCs are inactive and (d) along *y*-axis, when TDCs are inactive and BDCs are active.

the microfactory floor [see Fig. 1(b)]. In this configuration, the drive cells located directly beneath the micro conveyor can be activated to drive the mobile cross structure of the conveyor. The advantage of this configuration is twofold, first, the smaller length of the drive coils in each cell reduces the overall resistance of the current carrying coils, which leads to lower energy loss due to Joule heating. Second, each cell can be independently controlled from the perspective to achieve different motion trajectories of multiple conveyors (e.g., conveyor P_1 and P_2) as shown in Fig. 1(b).

In this paper, a new electromagnetic conveyor is presented. The proposed design allows the mobile part to travel in the plane at centimeter level displacement strokes. Its design and the working principle are described in Section II. An analytical electromagnetic model has been used to size the device and is provided in Section III. In Sections IV and V, the experimental setup and experimental results using a single mobile part along two axes are presented, respectively, to validate the long range motion capability of the conveyor. At the end, the conclusion and the perspectives regarding the proposed conveyor are provided.

II. Planar Electromagnetic Conveyor Architecture

This section describes the working principle of the planar electromagnetic conveyor and its detailed architecture with the help of three-dimensional models.

A. Working Principle

The working principle of the planar electromagnetic conveyor is based on generation of the electromagnetic forces (i.e., Lorentz forces). In order to do so, a pair of two $\pi/2$ phase shifted independent sinusoidal currents (I_1, I_2) and (I_3, I_4) are injected in top drive coils (TDCs) and bottom drive coils (BDCs), respectively, [see Fig. 1(c) and (d)]. Each TDCs and BDCs consists of a pair of fixed serpentine planar coils oriented along y- and x-axis, respectively. In addition, TDCs and BDCs are situated in first and second layer of the fixed part of the conveyor to ensure insulation. Due to the interaction between the injected currents I_1, I_2 in the TDCs (with no currents in the BDCs) and magnetic field generated by the mobile permanent magnet array (PMA) that consists of PMs assembled in north–south configuration, a translation force F_x and levitation force F_z appear [see Fig. 1(c)]. In similar fashion, if BDCs are injected with sinusoidal currents I_3, I_4 (with no currents in the TDCs), a translation force F_y and levitation force F_z appears [see Fig. 1(d)]. In both scenarios, the total levitation force component of the generated electromagnetic force (along z-axis) aids in compensating the weight of the mobile PMA, whereas the total translation force component helps the mobile PMA to move over the fixed part along an axis [see Fig. 1(c) and (d)].

The combination of the two fixed planar coils (i.e., TDCs and BDCs) and the mobile PMA acts as two-phase synchronous linear motor [19]. In the presented planar electromagnetic conveyor, a pair of two linear motors along x- and y-axis, respectively, aids the mobile part of the planar electromagnetic conveyor to move over the fixed part. The detailed architecture of the planar electromagnetic conveyor is described in the following section.

B. Planar Electromagnetic Conveyor Architecture

The planar electromagnetic conveyor design architecture consists of a mobile part and a fixed part [see Fig. 2(b)]. The mobile part includes four orthogonally arranged PMAs that are fixed at the extremities of a microfabricated silicon cross structure. The distance between the four PMAs (50 mm) ensures that the magnetic interaction force between the PMAs is in the order of 10^{-9}mN so it was neglected. Moreover, a single PMA is constructed with 14 Neodymium–Iron–Boron PMs.

Each PM has a cross section $(h \times w)$ of 1 mm $\times$ 0.5 mm and length l of 6 mm. Furthermore, each PM has the remanent magnetization of 1.43 T with the magnetization direction oriented along its thickness (i.e., h) in z-axis as shown in Fig. 2(a). The mechanical cross structure (having dimensions 68 mm $\times$ 68 mm $\times$ 0.5 mm and mass 3.6 g) was fabricated in the silicon material using microfabrication technology to achieve

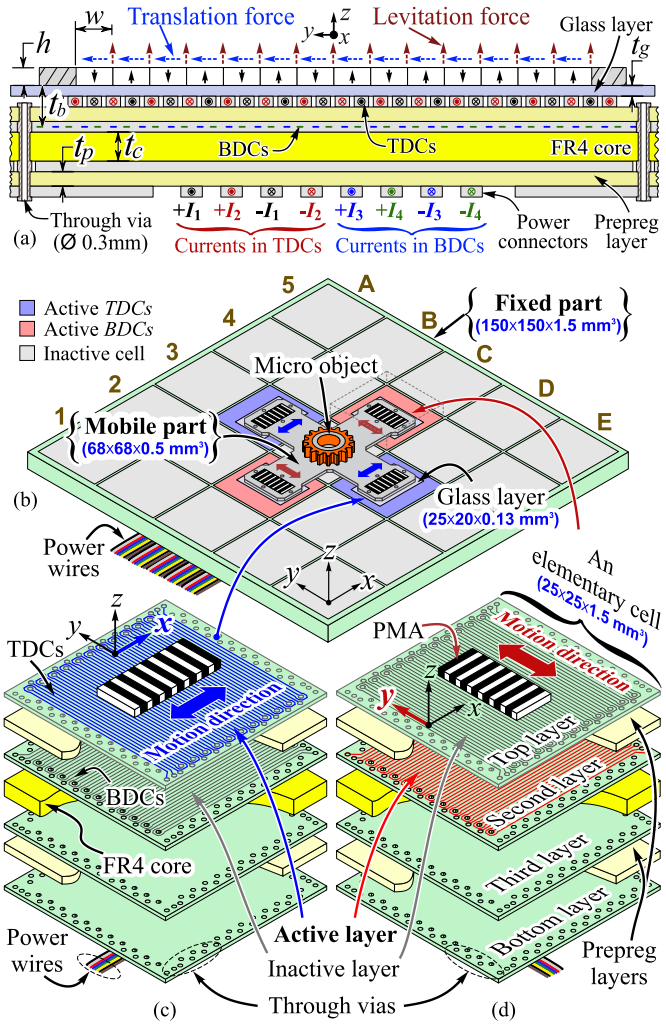

Fig. 2. (a) Cross-sectional view of a single linear motor. (b) Three-dimensional model view of the planar electromagnetic conveyor architecture composed of 5×5 elementary cells. Exploded view of the four layers of an elementary cell (c) with active TDCs to drive the PMA along x-axis (i.e., cell D3) and (d) with active BDCs to drive the PMA along y-axis (i.e., cell C4).

optimal design characteristics such as light weight, fabrication tolerances, etc., and to minimize assembly errors [17]. In addition, four glass layers each having thickness t_g of 130 μm were glued beneath the PMAs of the mobile part for insulation and achieve smooth motion surface.

The fixed part of the planar electromagnetic conveyor integrates 25 elementary drive cells distributed in a 5×5 matrix (i.e., rows: A, B, C, D, E and columns: 1, 2, 3, 4, 5) configuration [see Fig. 2(b)]. A single elementary drive cell (e.g., C2) consists of four-layer design and has a foot print of 25 mm $\times$ 25 mm. It includes a TDCs and a BDCs in top layer and second layer, respectively [see Fig. 2(c) and (d)]. Each TDCs (BDCs) integrates two 35 μm thick independent serpentine planar coils that enables the injection of $\pi/2$ phase shifted sinusoidal current I_1 (I_2) and I_3 (I_4), respectively. In addition, both TDCs (BDCs) are orthogonally oriented with respect to each other in their respective layers. In this manner, TDCs (BDCs) can be used independently to drive the mobile part of the planar electromagnetic conveyor by enabling the generation of electromagnetic forces through the pair of linear motors along x-axis (y-axis), respectively [4].

The fixed part design of the planar electromagnetic conveyor was commercially fabricated in a 150 mm $\times$ 150 mm $\times$ 1.5 mm four-layer printed circuit board (PCB) to avoid assembly errors between the 25 elementary cells that can appear if each elementary cell has been individually fabricated and assembled [17]. In order to insulate the four layers from each other, two prepreg layers (also known as preimpregnated layer, which is fibreglass impregnated with resin) along with an FR4 sheet having a thickness t_c of 0.9 mm as a central core for rigidity were employed in the design [see Fig. 2(c)]. In addition, the thickness t_p of 245 μm for the prepreg layers and a thickness of 35 μm for copper wires were used as fabrication standards to minimize the air gap t_b to 410 μm, which also includes the glass layer thickness t_g of 130 μm [see Fig. 2(a)]. To inject the external sinusoidal current such as $I_1(I_2)$ in TDCs and $I_3(I_4)$ in BDCs, the input/output terminals of the serpentine coils were routed through vias to the connecting pads in the bottom layer [see Fig. 2(a)]. In the third layer of the fixed part design, no copper routes were placed except through vias that links all layer to the bottom side. This layer acts as a dummy layer and is present due to the fabrication constraint. However, this additional layer aids in increasing the air gap between the bottom layer and PMA, thus minimizing the parasitic noise that can appear due to the currents at the bottom side [20].

III. Modeling and Analysis

In the following section, an analytical model is presented for a single linear motor due to the symmetry of the design. However, the solution has been extended to take into account the whole planar electromagnetic conveyor for the simulation purpose. In addition, the influence of some fabrication constraints imposed by the chosen architecture have been studied and analyzed to evaluate their effect on the conveyor performances.

A. Magnetic Flux Density Computation Model

The magnetic flux density generated by a PMA is modeled by reducing the 14 PMs to their equivalent current distribution. Some assumptions are taken into account that include perfect geometry of the PMs, no variation in magnetization of each PM along its length, and identical magnetization characteristics of each PM in a PMA [6]. With these assumptions, the magnetic flux density distribution at any point (x, z) outside the PMA [for the case where the PMs are oriented along y-axis as shown in Fig. 2(c)] is computed using (1). The origin of the reference frame is located at the center of the PMA and the B_x and B_z represents the horizontal and vertical components of the magnetic flux density, respectively [21]. The B_y component of the magnetic flux density has been neglected because of its small contribution ($\approx 10^{-12}$ mT) as compared to the contribution of B_x and B_z.

Where, M_s is the magnetization of the PM in A/m and μ_0 is the magnetic permeability of air in N/A^2, a and b are the half values of the width ($w/2$) and height ($h/2$) of a PM in m,

respectively [see Fig. 2] as

$$B_x = \frac{\mu_0 M_s}{4\pi}\left[2\sum_{i=1}^{14}\ln\left(\frac{(x-2ia)^2+(z-b)^2}{(x-2ia)^2+(z+b)^2}(-1)^i\right) - \ln\left(\frac{(x-28a)^2+(z-b)^2}{(x-28a)^2+(z+b)^2}\right) - \ln\left(\frac{(x+a)^2+(z-b)^2}{(x+a)^2+(z+b)^2}\right)\right]$$

$$B_z = \frac{\mu_0 M_s}{4\pi}\left[2\sum_{i=1}^{14}a\tan\left(\frac{2b(x-2ia)(-1)^i}{(x-2ia)^2+z^2-b^2}\right) - a\tan\left(\frac{2b(x-28a)}{(x-28a)^2+z^2-b^2}\right) - a\tan\left(\frac{2bx}{(x-2a)^2+z^2-b^2}\right)\right]. \quad (1)$$

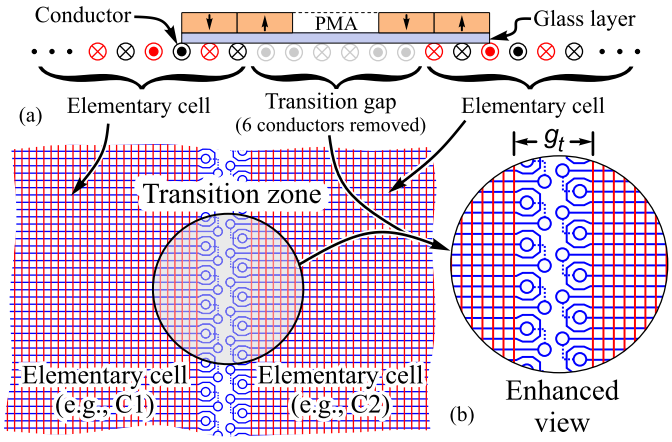

Fig. 3. (a) PMA over the 3.5 mm transition gap generated by removing six current carrying conductor. (b) Pictorial view of the transition zone between two adjacent elementary drive cells (e.g., C1 and C2) of the planar electromagnetic conveyor.

B. Electromagnetic Force Computation Model

As discussed in previously, the electromagnetic force (or Lorentz force) appears along x- and y-axis by injecting $I_1(I_2)$ and $I_3(I_4)$ in TDCs and BDCs, respectively. The total electromagnetic force $\mathbf{F}_{\text{total}}$ generated due to each drive coils by a single linear motor is computed using (2) [21]

$$\mathbf{F}_{\text{total}} = \underbrace{N_t\sum_{k=1}^{2}\mathbf{I}_k\int_{\text{wire}} dl\times\mathbf{B}_{\text{ext}}^{(k)}}_{\text{with TDCs}} + \underbrace{N_b\sum_{q=1}^{2}\mathbf{I}_q\int_{\text{wire}} dl\times\mathbf{B}_{\text{ext}}^{(q)}}_{\text{with BDCs}} \quad (2)$$

where $\mathbf{B}_{\text{ext}}$ is the external magnetic flux density computed using (1). N_t and N_b denote the number of turns in the current carrying coil of TDCs and BDCs, respectively. The parameters k and q denote the relative position index for the magnetic flux density computation with respect to the current carrying coils in TDCs and BDCs of the fixed part, respectively. Furthermore, $\mathbf{I}_k$ and $\mathbf{I}_q$ represent the magnitude of the sinusoidal current in the respective coils.

The choice of sinusoidal injected currents was made due to the fact that the magnetic field generated by the PMs is nearly sinusoidal with respect to the relative position between PMA and current carrying conductors. Indeed, this leads to small variations in the generated electromagnetic force, which induce small nonlinearities during displacements of the mobile part. However, this choice was made to facilitate the arrangement of small PMs in an array form. Nevertheless, the influence of the aforementioned nonlinearities are very small comparative to the mobile part's long-range motion.

C. Transition Zone Analysis

From Fig. 2(b), it can be seen that the elementary cells are distributed in a matrix configuration. However, in reality, this design configuration introduced a fabrication constraint to accommodate through vias between adjacent elementary cells. These vias are used to connect TDCs and BDCs to the bottom layer side of the PCB. The placement of through vias lead to a transition gap g_t between adjacent elementary cells as shown in the enhanced view of Fig. 3(b). As a result of this transition gap, a loss in generated electromagnetic forces (i.e., translation and levitation forces) is experienced by the mobile part, when the PMAs enters in this zone during motion.

In order to quantify the aforementioned force loss in the transition zone, a static analysis with a semi-analytical software RADIA has been realized during the design phase of the fixed part of the conveyor. This study has been conducted by removing a pair of conductors each time to generate a transition gap g_t [see Fig. 3(a)] and then injecting currents having amplitude of 0.4 and 0.8 A in the TDCs and the BDCs, respectively. These current values were selected to achieve same order of the magnitude for the translation forces during motion along x- and y-axis.

The evolution in the magnitude of the translation and levitation forces generated by a single linear motor in the transition zone is shown in Fig. 4. From the results, it can be observed that in ideal case (when no conductor is removed), the maximum values of the translation (levitation) forces are found to be 13.75 mN (21.03 mN) using TDCs and 13.94 mN (12.96 mN) using BDCs, respectively. The difference between the force values computed for TDCs and BDCs are due to the different air gap values between the current carrying conductors in the top and second layer of the fixed part and the PMA of the mobile part [i.e., $t_g = 130\,\mu$m for TDCs and $t_b = 410\,\mu$m for BDCs, see Fig. 2(a)].

In our planar electromagnetic conveyor design, six conductors have been removed in TDCs and BDCs to yield a transition gap g_t of 3.5 mm between adjacent elementary cells of the fixed part for placing through vias (each having hole diameter of 300 μm), to overcome the commercial fabrication constraints [see Fig. 3]. This transition gap resulted in a loss of 21.45% in the translation and levitation forces generated by a single linear motor when using either TDCs or BDCs. However, even with this loss, the generated translation force is enough to translate the mobile part over the fixed part of the conveyor. The vertical electromagnetic

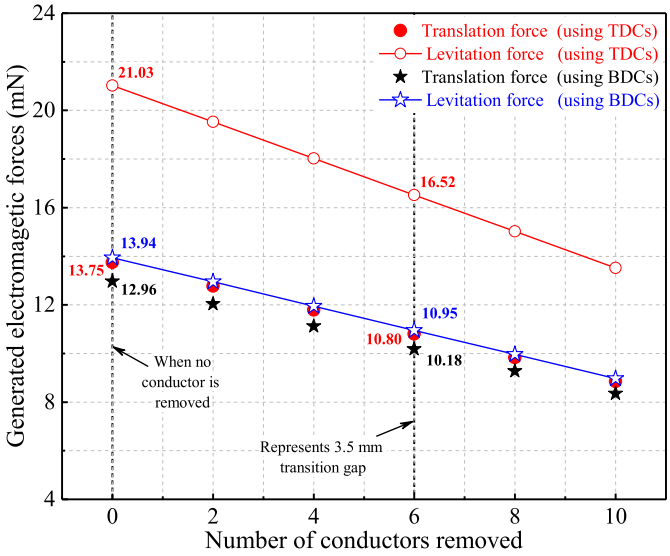

Fig. 4. Translation and levitation forces generated by an linear motor in the transition zone between two adjacent elementary cells by removing 0, 2, 4, 6, 8, 10 current carrying conductors in TDCs and BDCs.

force component acts against the weight of the mover (35 mN) but is not sufficient enough to levitate it.

D. Mechanical Model

The mechanical model takes into the account the total electromagnetic forces F_{total} and friction force F_f between the mobile part and the fixed part of the conveyor during motion. The total electromagnetic force is the sum of the electromagnetic forces generated by all four linear motors. The friction force is computed using $F_f = W_{\text{net}} \times \mu_f = (mg - F_{\text{total}_z}) \times \mu_f$, where W_{net} is the net weight of the mobile part, m is the mass of the mobile part, F_{total_z} is the total electromagnetic force component along z-axis, and μ_f is the friction coefficient interpreted as static μ_s or dynamic μ_d during motion. The values of static friction coefficient $\mu_s = 0.23$ and dynamic friction coefficient $\mu_d = 0.21$, were experimentally measured using inclined plane technique [22]. Then, the mobile part's displacement d is computed by double integration of the acceleration as given by

$$\begin{bmatrix} dx \\ dy \end{bmatrix} = \frac{1}{m} \begin{bmatrix} \int\int (F_{\text{total}_x} - F_f) dt dt \\ \int\int (F_{\text{total}_y} - F_f) dt dt \end{bmatrix} \tag{3}$$

where d_x, d_y are the mobile part's displacement and F_{total_x}, F_{total_y} are the total electromagnetic force components computed along x- and y-axis using (2), respectively.

IV. Experimentation

In this section, the experimental setup of the planar electromagnetic conveyor is presented. Furthermore, the displacement measurement using image processing with MATLAB software is described.

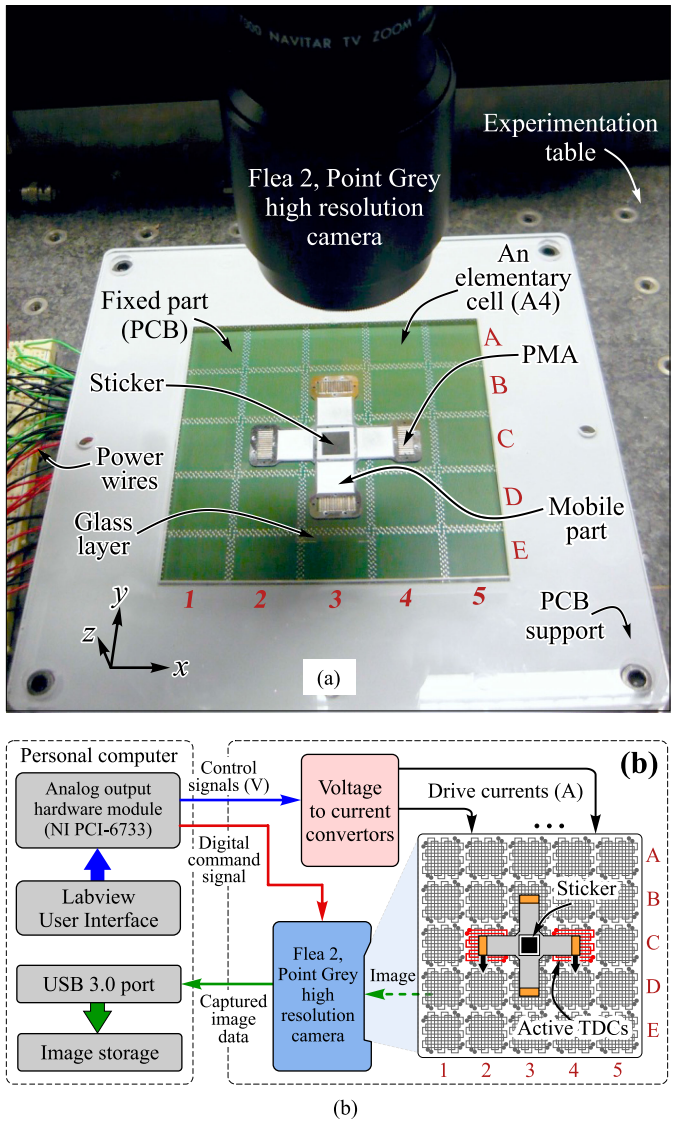

Fig. 5. (a) Real view of the planar electromagnetic conveyor design showing different elements of the experimental setup. (b) Block diagram of the hardware/software interface.

A. Description of the Experimental Setup

The experimental setup has been realized by first, assembling four PMAs into the through cavities of a silicon cross structure to form the mobile part. Then, four 130 μm glass layers were glued beneath each PMA to insulate and achieve a smooth surface in between the mobile and fixed part of the conveyor. In order to ensure proper mounting of the conveyor on experimentation table, a PCB support has been fabricated in a 5-mm thick acrylic glass sheet [see Fig. 5(a)]. Moreover, in order to measure the mobile part's centimeter level displacement while avoiding any external contact during motion, an image processing based solution has been adopted by installing a high resolution camera (Grasshopper 3, Point Grey Inc.) over the conveyor platform [see Fig. 5(a)]. In addition, a black square printed on a white sticker was glued at the center of the mobile part to facilitate

better interpretation of captured images for the displacement measurement process. Afterwards, the high-resolution camera was calibrated and the pixel resolution was found to be 45 μm. This limits the measurement of the displacement realized by the mobile part to 45 μm. In our previous study [17], a minimum step size of 2 μm was reported using high resolution optical displacement sensor (i.e., 8 nm). This sensor was not employed in this study due to its maximum displacement measurement range of 2.5 mm.

The hardware/software connectivity is presented in the Fig. 5(b). A dedicated Labview program was developed to deliver voltage control signals using a 16-bit PCI 6733 analog hardware module developed by National Instruments. These control signals [range: +10 V, −10 V] were delivered to two pairs of two voltage-to-current (V/I) convertors to inject sinusoidal currents into the TDCs and BDCs, independently. As a result, the desired respective elementary cells of the planar electromagnetic conveyor were activated to drive the mobile part along x- axis and/or y-axis. The motion of the mobile part over the fixed part of the planar electromagnetic conveyor was captured with the help of the installed high-resolution camera. A synchronization between the conveyor control and the image capturing process was realized using a digital command signal provided to the camera through Labview interface. Each captured image was stored in the personal computer for mobile part's displacement measurement analysis.

B. Displacement Measurement via Image Processing

The captured high-resolution images during experimentation were processed using image processing technique to measure the displacement realized by the mobile part. In order to reduce the image processing time of n numbers of images and improve pixel detection resolution of the camera, the images were taken over a specific region of the mobile part, mainly focusing on the desired detection area i.e., the black sticker. Also, the image capturing sequence has been realized at a rate of 30 fps over a translation distance of 50 mm. So, in order to process the captured images, an image processing algorithm has been developed using MATLAB to detect the square shape of the black sticker to measure the respective location of the mobile part of the conveyor. The different image processing steps are presented in Fig. 6. Initially, the saved images (i.e., $\alpha_{i\ldots n}$) are read one by one and converted from RGB image to binary image (i.e., α_{i_b}) by setting the pixel threshold value to 1(0) representing white(black), respectively. Then, in the next step, the binary image is filtered by removing objects that are composed of few pixels and a new binary image is created (i.e., α_{i_nb}). The boundaries of the remaining objects in the new binary image are then detected and traced to form different areas. The desired square area of the black sticker (10 mm × 10 mm) is then searched and its centroid's xy-coordinates are retrieved. This process is repeated for n number of captured images.

V. Results and Discussion

In this section, different results obtained via experimentations are presented. These results have been obtained in open loop by injecting sinusoidal currents of 0.4 and 0.8 A in TDCs and BDCs to drive the mobile part over the conveyor platform along x-axis and y-axis, respectively.

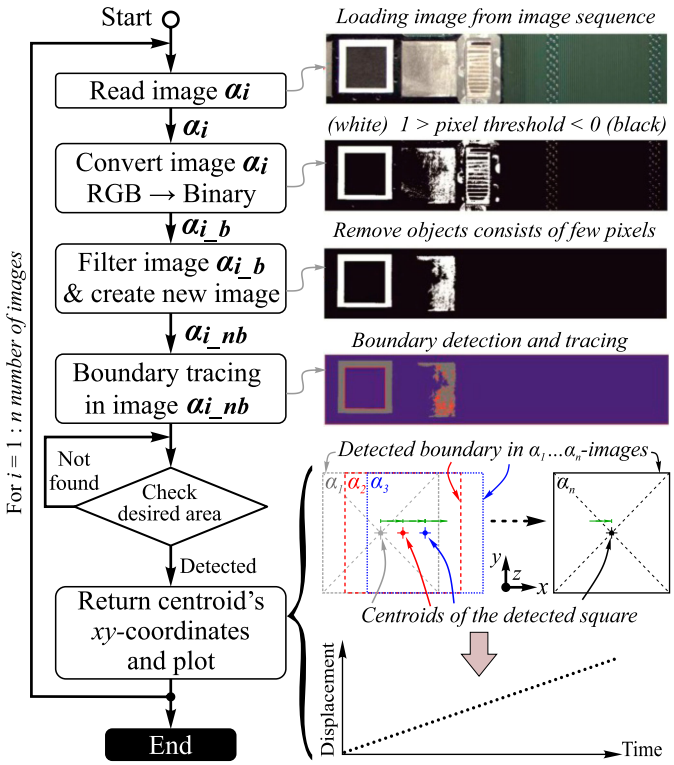

Fig. 6. Schematic layout of the image processing algorithm developed in MATLAB to identify the square shape and to calculate the displacement of its centroid in xy plane.

A. Linear Displacement Along a Single Axis

Linear displacements along x-axis and y-axis realized by the mobile part are presented in Fig. 7. In order to actuate the mobile part of the conveyor along x-axis, the TDCs beneath the PMAs of the mobile part were activated by injecting 0.4 A sinusoidal currents to achieve 50 mm travel distance. Meanwhile, the BDCs beneath the PMAs of the mobile part were in idle state (i.e., no current was injected). In similar fashion, to drive the mobile part along y-axis, respective BDCs of the elementary cells beneath the PMAs of the mobile part were activated while TDCs were in idle state. The linear displacement results along two axes were obtained at different speeds by changing the sampling frequency of the injected currents in TDCs and BDCs. In practice, a period of the sinusoidal current is sampled to achieve theoretical displacement of 2 mm, which corresponds to the pitch of the PMA (i.e., 2 mm). So, the actuation speed is proportional to the sampling frequency. The experiment along y-axis was conducted at 4 mm/s (i.e., 2 Hz sampling frequency) whereas, along x-axis it was carried out at 2 mm/s (i.e., 1 Hz sampling frequency). This speed variation criterion for the experiment was adapted because of two reasons. First, to demonstrate that the mobile part could perform motion at different speeds and second to minimize the generation of the Joule heating using BDC. For

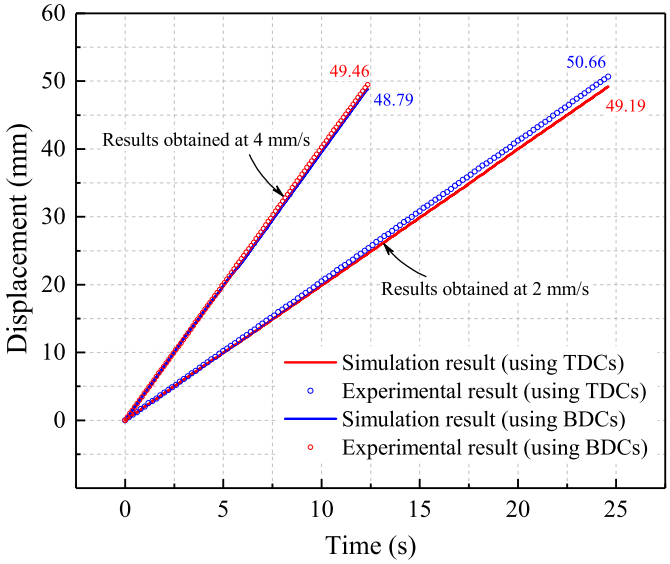

Fig. 7. Experimental and simulation results of the linear displacement of the mobile part obtained at 2 and 4 mm/s along x- and y-axis, respectively.

the same current value, the Joule heating is higher using BDC than TDC due to the fact that BDC is inside the PCB. However, to minimize the Joule heating effect using BDC, the motion has been performed at higher speed to minimize the current injection time [19].

Furthermore, a comparative study was conducted to validate the simulation model. So, for a desired linear displacement of 50 mm, the simulated 49.19 mm (48.79 mm) and the experimental 50.66 mm (49.46 mm) results were obtained along x-axis (y-axis), respectively. From these results, it can be observed that the mobile part travels over multiple elementary cells. Furthermore, the small variation between the simulated and experimental results was due to the variation in the adhesion forces and drift effect during the motion of the mobile part. Nevertheless, in Fig. 7, a good agreement can be observed between results along the both displacement axes.

B. Position Repeatability in Linear Displacement

A position repeatability test has been conducted to investigate the behavior of the planar electromagnetic conveyor in repetitive motion. Three cycles of long range displacement (i.e., 70 mm) along x-axis by injecting currents in the TDCs of the conveyor has been carried out. Fig. 8, shows the displacement realized by the mobile part along x-axis in a three cycles test obtained at 2 mm/s speed. From the result, along y-axis, a repeatable drift effect interpreted here as straightness error can be observed. For a measured displacement of 69.48 mm realized by the mobile part along x-axis, the position repeatability error was found to be 6.8 μm. In addition, the straightness error due to the parasitic displacement along y-axis was found to be 65 μm with a standard deviation of 3.7 μm. This error is due to the fact that there is no guidance of the mobile part during motion.

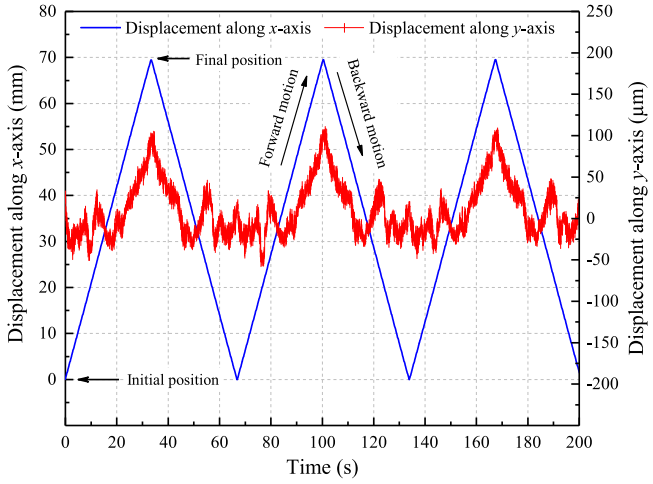

Fig. 8. Three cycles of the forward and backward motion of the mobile part at 2 mm/s speed along x-axis along with the straightness error along y-axis.

C. Influence of the Guidance Current on Straightness Error

The interesting feature reported earlier in [6] is that the north–south configuration of the PMs in the PMA aids in aligning the mobile part of the conveyor with respect to the current carrying conductors. This alignment feature is achieved by injecting constant current (here called guidance current) along x-axis (i.e., in TDCs) during motion along y-axis using BDCs and vice versa. To investigate the influence of the guidance current during linear motion, a study has been conducted by driving the mobile part at 12 mm/s speed along x-axis using TDCs and injecting constant current in BDCs. A motion speed of 12 mm/s was selected for this test to clearly observe the influence of the guidance current, which was not visible at lower motion speed. From the result presented in Fig. 9, it can be seen that with no guidance current the mobile part exhibits a drift effect of 184 μm along y-axis for a 70 mm translation along x-axis. After subtracting slope due to this drift effect, the straightness error was found to be 68.73 μm. However, by increasing the magnitude of the guidance current, i.e., $\geq$ 0.1 A, the straightness error is significantly reduced to 7.53 μm.

D. Linear Displacement in the xy Plane

In order to achieve linear displacement in the xy plane, sinusoidal currents are injected in both TDCs and BDCs of the conveyor. As a result, the linear displacement realized by all four linear motors helps the mobile part to translate in xy plane over the fixed part of the conveyor. This test has been conducted at different speeds (i.e., 4, 8, and 12 mm/s) by changing the sampling frequency of the injected sinusoidal currents. Fig. 10 represents the forward and backward motion realized by the mobile part between position A and position C at the above-mentioned speeds. A good repeatable trajectory motion realized by the mobile part can be observed. The small deviation

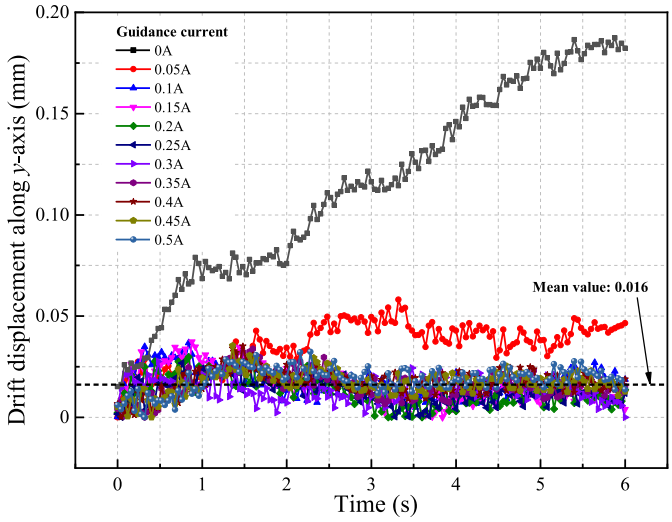

Fig. 9. Influence of the guidance currents injected in BDCs to reduce the straightness error along y-axis during linear motion along x-axis at 12 mm/s.

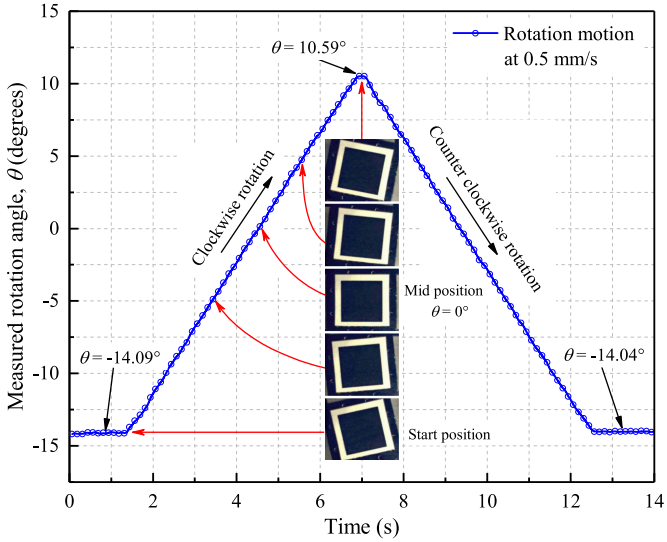

Fig. 11. Rotation motion realized by the mobile part of the planar electromagnetic conveyor about its center in xy plane.

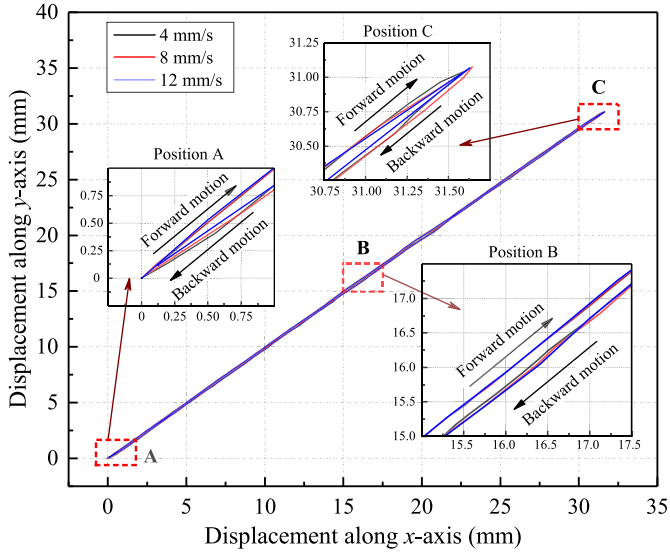

Fig. 10. Linear motion realized by the mobile part in xy plane at different speeds and their enhanced view.

between the forward and backward motion trajectory as shown in the enhanced view of position B, is due to aforementioned drift effect.

E. Rotation Motion

Rotation motion of the mobile part has been achieved by reversing the direction of injected currents in the elementary cells situated beneath the PMAs along each axis. As a result, the generated forces are in opposite directions, which rotates the mobile part about its center in xy plane. To measure the rotation motion realized by the mobile part, a lens (infinity probes) was used with the aforementioned high-resolution camera. This choice has been made to improve the limit of the resolution of the pixel (found to be 7 μm) by minimizing the field of view to 17 mm $\times$ 14 mm, mainly focusing on the black square as shown in the Fig. 11. Several images were captured by the camera during motion with the time delay of 0.0625 s between each image. The image processing algorithm has been then used to measure the rotation angle of the black square [see Fig. 11].

The rotation motion experiment has been conducted at a speed of 0.5 mm/s and the maximum measured angle was found to be 24.5°. Moreover, at different speeds (i.e., 1, 2, and 3 mm/s) the average value of the maximum rotation range was found to be $\pm$12.37° about center of the mobile part in xy plane. This rotation range value is limited because of the geometrical limits of the elementary cells.

VI. Conclusion

In this paper, a planar electromagnetic conveyor is presented. The conveyor architecture includes 25 independently controlled elementary cells arranged in a 5 $\times$ 5 matrix configuration. This architecture enables the mobile part to perform long displacement strokes (i.e., 69.48 mm) and planar motions at variable speeds up to 12 mm/s with 0.8 A nominal controlling current. The conveyor architecture enables a guidance function that limits the straightness error to 7.53 μm in a 70 mm displacement stroke by injecting a guidance current ($\geq$0.1 A). Further, the maximum rotation range of the mobile part has been measured to be $\pm$12.37° about the center of the mobile part in xy plane.

One of the potential applications is to realize a large microfactory floor to move multiple micro parts between different micromanufacturing stations. Indeed, the proposed conveyor design allows to control several mobile parts simultaneously and the motion trajectories of these mobile parts can be easily programmed, which enables high and/or flexible production flow. Another application is to use the proposed design in scanning microscopy domain to move micromachined parts beneath surface scanning equipment for long range characterization.

References

[1] R. Pérez, O. Dávila, A. Molina, and M. Ramírez-Cadena, "Reconfigurable micro-machine tool design for desktop machining microfactories," in *Proc. 7th IFAC Conf. Manuf. Modelling, Manage., Control*, vol. 46, 2013, pp. 1417–1422. [Online]. Available: http://www.Sciencedirect.com/science/article/pii/S1474667016344913

[2] Y. Okazaki, "Microfactories—A new methodology for sustainable manufacturing," *Int. J. Autom. Technol.*, vol. 4, no. 2, pp. 82–87, 2010.

[3] Z. Zhakypov, T. Uzunovic, A. O. Nergiz, E. A. Baran, E. Golubovic, and A. Sabanovic, "Desktop microfactory for high precision assembly and machining," in *Proc. IEEE 23rd Int. Symp. Ind. Electron.*, Jun. 2014, pp. 1192–1197.

[4] T. A. T. Dang, M. Bosch-Mauchand, N. Arora, C. Prelle, and J. Daaboul, "Electromagnetic modular smart surface architecture and control in a microfactory context," *Comput. Industry*, vol. 81, no. Supplement C, pp. 152–170, 2016. [Online]. Available: http://www.sciencedirect.com/science/article/pii/S0166361516300033

[5] S. Scheifele, J. Friedrich, A. Lechler, and A. Verl, "Flexible, self-configuring control system for a modular production system," *Proc. Technol.*, vol. 15, no. Supplement C, pp. 398–405, Feb. 2014.

[6] M. U. Khan, N. Bencheikh, C. Prelle, F. Lamarque, T. Beutel, and S. Buttgenbach, "A long stroke electromagnetic *XY* positioning stage for micro applications," *IEEE/ASME Trans. Mechatronics*, vol. 17, no. 5, pp. 866–875, Oct. 2012.

[7] R. Yahiaoui, R. Zeggari, J. Malapert, and J.-F. Manceau, "A MEMS-based pneumatic micro-conveyor for planar micromanipulation," *Mechatronics*, vol. 22, no. 5, pp. 515–521, 2012. [Online]. Available: http://www.sciencedirect.com/science/article/pii/S0957415811001012

[8] M. Ataka, B. Legrand, L. Buchaillot, D. Collard, and H. Fujita, "Design, fabrication, and operation of two-dimensional conveyance system with ciliary actuator arrays," *IEEE/ASME Trans. Mechatronics*, vol. 14, no. 1, pp. 119–125, Feb. 2009.

[9] Y. Li and Q. Xu, "Development and assessment of a novel decoupled *XY* parallel micropositioning platform," *IEEE/ASME Trans. Mechatronics*, vol. 15, no. 1, pp. 125–135, Feb. 2010.

[10] W. Rong, S. Liang, L. Wang, S. Zhang, and W. Zhang, "Model and control of a compact long-travel accurate-manipulation platform," *IEEE/ASME Trans. Mechatronics*, vol. 22, no. 1, pp. 402–411, Feb. 2017.

[11] T. Hosobata, A. Yamamoto, and T. Higuchi, "Transparent synchronous electrostatic actuator for long-stroke planar motion," *IEEE/ASME Trans. Mechatronics*, vol. 20, no. 4, pp. 1765–1776, Aug. 2015.

[12] Y. Fukuta, Y. A. Chapuis, Y. Mita, and H. Fujita, "Design, fabrication, and control of MEMS-based actuator arrays for air-flow distributed micromanipulation," *J. Microelectromech. Syst.*, vol. 15, no. 4, pp. 912–926, Aug. 2006.

[13] V. Guelpa, G. J. Laurent, B. Dahroug, and N. L. Fort-Piat, "Modular contact-free conveyors for handling planar fragile objects," *IEEE Trans. Robot.*, vol. 33, no. 1, pp. 92–101, Feb. 2017.

[14] M. Lahdo, T. Ströhla, and S. Kovalev, "Repulsive magnetic levitation force calculation for a high precision 6-DoF magnetic levitation positioning system," *IEEE Trans. Magn.*, vol. 53, no. 3, Mar. 2017, Art. no. 7200106.

[15] V. H. Nguyen and W. J. Kim, "Design and control of a compact lightweight planar positioner moving over a concentrated-field magnet matrix," *IEEE/ASME Trans. Mechatronics*, vol. 18, no. 3, pp. 1090–1099, Jun. 2013.

[16] J. L. Perez-Diaz, I. Valiente-Blanco, E. Diez-Jimenez, and J. Sanchez-Garcia-Casarrubios, "Superconducting noncontact device for precision positioning in cryogenic environments," *IEEE/ASME Trans. Mechatronics*, vol. 19, no. 2, pp. 598–605, Apr. 2014.

[17] M. U. Khan, C. Prelle, F. Lamarque, and S. Büttgenbach, "Design and assessment of a micropositioning system driven by electromagnetic actuators," *IEEE/ASME Trans. Mechatronics*, vol. 22, no. 1, pp. 551–560, Feb. 2017.

[18] Q. Xu, "Design and development of a compact flexure-based XY precision positioning system with centimeter range," *IEEE Trans. Ind. Electron.*, vol. 61, no. 2, pp. 893–903, Feb. 2014.

[19] M. U. Khan, A. Charvet, J. Terrien, F. Lamarque, and C. Prelle, "Design and thermal assessment of a micro electromagnetic actuator," in *Proc. 11th France-Japan 9th Europe-Asia Congr. Mechatronics/17th Int. Conf. Res. Educ. Mechatronics*, Jun. 2016, pp. 260–265.

[20] N. Arora, M. U. Khan, L. Petit, and C. Prelle, "A planar electromagnetic actuator based on two layer coil assembly for micro applications," in *Proc. IEEE/ASME Int. Conf. Adv. Intell. Mechatronics*, Jul. 2014, pp. 174–179.

[21] E. P. Furlani, *Permanent Magnet and Electromechanical Devices—Materials, Analysis and Applications*. San Diego, CA, USA: Academic, 2001, pp. 208–216.

[22] L. Petit, H. A. Hajjar, C. Prelle, and F. Lamarque, "Design, modeling, and characterization of an optical switch based on four positions digital actuator," *IEEE/ASME Trans. Mechatronics*, vol. 21, no. 3, pp. 1518–1527, Jun. 2016.

Neha Arora received the Ph.D. degree in mechanical engineering with specialization in mechatronic systems from Université de Technologie de Compiègne, Compiègne, France, in 2017.

She is currently a Research Engineer. Her research interest includes microsystem design and microfactories.

Muneeb Ullah Khan received the double Ph.D. degrees in mechanical engineering with the specialization in microsystem design from Université de Technologie de Compiègne, Compiègne, France, and Institute for Microtechnology, Technische Universität Braunschweig, Braunschweig, Germany, in 2014.

He is currently a Research Engineer with Roberval Laboratory, Université de Technologie de Compiègne, Compiègne, France. His research interest includes microactuators, microsensors, and micromechatronic system designs.

Laurent Petit received the Ph.D. degree in mechanical engineering from Université de Technologie de Compiègne, Compiègne, France, in 2009.

He is currently an Associate Professor in mechanical and mechatronics engineering with Roberval Laboratory, Université de Technologie de Compiègne, Compiègne, France. He is a member of the Laboratory of Excellence "Control of Technological Systems-of-Systems" (labex MS2T). His research interests include mechatronic systems, compact electromagnetic actuators, and digital actuation.

Frédéric Lamarque received the Ph.D. degree in electronics from Université Paris Sud, Orsay, France, in 1998.

He is currently a Professor in sensors and instrumentation with Roberval Laboratory, Université de Technologie de Compiègne, Compiègne, France. He is a member of the Laboratory of Excellence "Control of Technological Systems-of-Systems" (labex MS2T). His research interest includes microsensors and microactuators.

Christine Prelle received the Ph.D. degree in industrial automatic control from Institut National des Sciences Appliquées Lyon, Villeurbanne, France, in 1997.

She is currently a Professor in control engineering and mechatronics with Roberval Laboratory, Université de Technologie de Compiègne, Compiègne, France. She is member of the Laboratory of Excellence "Control of Technological Systems-of-Systems" (labex MS2T). She is currently In-Charge of the Doctoral School "Science for engineers," Université de Technologie de Compiègne, Compiègne, France. Her research interest includes micromechatronics and control.